Position and motions of the S4 helix during opening of the Shaker potassium channel

L. Revell Phillips and Kenton J. Swartz

Molecular Physiology and Biophysics Section, Porter Neuroscience Research Center, National Institutes of Neurological Disorders and Stroke, National Institutes of Health, Bethesda, MD 20892

The four voltage sensors in voltage-gated potassium (Kv) channels activate upon membrane depolarization and open the pore. The location and motion of the voltage-sensing S4 helix during the early activation steps and the final opening transition are unresolved. We studied Zn^{2+} bridges between two introduced His residues in Shaker Kv channels: one in the R1 position at the outer end of the S4 helix (R362H), and another in the S5 helix of the pore domain (A419H or F416H). Zn^{2+} bridges readily form between R362H and A419H in open channels after the S4 helix has undergone its final motion. In contrast, a distinct bridge forms between R362H and F416H after early S4 activation, but before the final S4 motion. Both bridges form rapidly, providing constraints on the average position of S4 relative to the pore. These results demonstrate that the outer ends of S4 and S5 remain in close proximity during the final opening transition, with the S4 helix translating a significant distance normal to the membrane plane.

The Journal of General Physiology

INTRODUCTION

Voltage-gated potassium (Kv) channels are present in all cells, and they fulfill a wide variety of important roles. In neurons and excitable cells, for example, Kv channels open and close in response to changes in membrane voltage and are involved in the generation and propagation of electrical signals (Hille, 2001). Kv channels are tetramers, with each subunit containing six membrane-spanning helices, termed S1 through S6 (Swartz, 2004). The channel pore is collectively formed by the S5 and S6 portions of each subunit and is surrounded by four voltage-sensing domains, each constructed from the S1–S4 portion of a single subunit (Long et al., 2007). Basic residues in the S4 helix of each voltage-sensing domain move in response to changes in voltage, producing a measurable gating current (Bezanilla, 2002) and driving the opening of the S6 gate located at the intracellular end of the pore (Yellen, 2002).

The gating mechanism of the Shaker Kv channel has been particularly well studied, with extensive evidence revealing that gating involves multiple early activation steps as the four voltage sensors move between resting (R) and activated (A) states, followed by a final opening transition where the S6 gate moves from a closed (C) to an open (O) state. This conceptual model (Scheme 1), taken from the work of Ledwell and Aldrich (1999), is supported by electrophysiological investigation of the wild-type and mutant Shaker Kv channels (Bezanilla et al., 1994; Hoshi et al., 1994; Stefani et al., 1994; Zagotta et al., 1994a,b; Schoppa and Sigworth, 1998a,b,c; Smith-Maxwell et al., 1998a,b; Ledwell and Aldrich, 1999; Sukhareva et al., 2003; del Camino et al., 2005; Pathak et al., 2005). The Shaker ILT mutant (V369I, I372L, and S376T) has been a particularly useful tool because the R to A steps occur at considerably more negative voltages compared with the final opening transition (Smith-Maxwell et al., 1998a,b; Ledwell and Aldrich, 1999). Although most of the gating charge in ILT moves during the early transitions between the R and A states, a significant

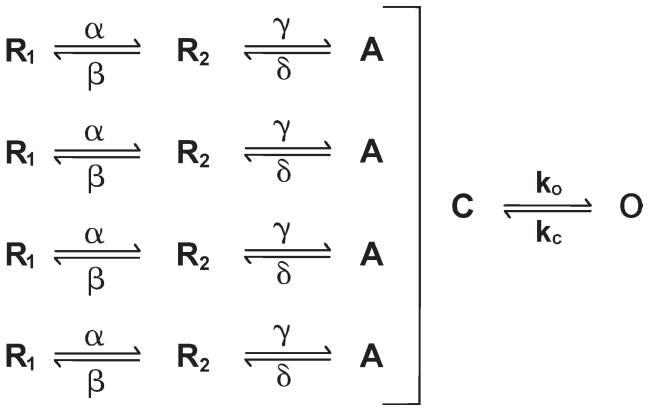

(SCHEME 1)

Correspondence to Kenton J. Swartz: swartzk@ninds.nih.gov

Abbreviations used in this paper: IR, inactivation removed; Kv, voltage-gated potassium.

The Rockefeller University Press $30.00
J. Gen. Physiol. Vol. 136 No. 6 629–644
www.jgp.org/cgi/doi/10.1085/jgp.201010517

gating charge can be measured during the final opening transition (Ledwell and Aldrich, 1999), raising the possibility that the voltage sensors might also move during the late opening transition. The strongest evidence to support this type of late S4 motion is that probes attached to the external end of the S4 helix exhibit fluorescence changes during the final opening transition (Pathak et al., 2005). Although voltage sensor movements may occur during both early and late steps in the gating of Shaker Kv channels, the position of the crucial S4 helix relative to other parts of the protein and the extent to which this helix moves during specific transitions remain unresolved. In addition, linking the x-ray structures of Kv channels to specific states in gating models obtained from functional experiments is not straightforward. The internal gate regions in the three Kv channel structures solved thus far appear to have been caught in an open state (Jiang et al., 2003; Long et al., 2005, 2007); however, more information is needed to understand how the voltage sensors in these structures relate to those in functional channels embedded in a native lipid environment, in particular, given the inherent flexibility of voltage sensors (Jiang et al., 2003; Cuello et al., 2004; Lee et al., 2005; Chakrapani et al., 2008; Vamvouka et al., 2008) and the growing appreciation for the influence of lipids on channel structure and function (Ramu et al., 2006; Schmidt et al., 2006; Milescu et al., 2007, 2009; Schmidt and MacKinnon, 2008; Xu et al., 2008).

Metal bridges between introduced cysteine (Cys) or histidine (His) residues offer a powerful approach to explore the position and motions of defined regions of proteins, as shown for the gate region of the Shaker Kv channel (Holmgren et al., 1998; Webster et al., 2004; del Camino et al., 2005), and more recently for P2X receptor channels (Li et al., 2010). Lainé et al. (2003) discovered that a Zn^{2+} bridge can form between two His residues introduced in Shaker channels: one at A419 in the extracellular end of the S5 helix in the pore domain, and the other at R362, the R1 position of the S4 helix within the voltage sensor. Zn^{2+} causes a leftward shift in the voltage–activation relationship for these channels, suggesting either an open-state stabilization or a closed-state destabilization. This bridge occurs in the presence of nanomolar concentrations of Zn^{2+}, indicating that the equilibrium affinity of Zn^{2+} is quite high. Similar results can be obtained in the Kv1.2 channel after neutralization of several acidic residues that are not present in Shaker (Lewis et al., 2008). One possibility is that the bridge occurs between residues that are in close proximity and thus might be expected to form rapidly (i.e., high on rate). Alternatively, the two His residues might only rarely encounter each other, a scenario in which the bridge would form slowly and the high affinity would result instead from a very low off-rate. Lainé et al. (2003) also examined metal bridges between Cys residues at F416 and R362. These metal bridges cause an apparent rightward shift in the voltage–activation relationship, suggesting either a closed-state stabilization or an open-state destabilization. In contrast, Broomand et al. (2003) found that disulphide bonds between these same two Cys residues do not form when channels are held closed at negative voltages, but do form when cells are repeatedly depolarized to open channels, leading them to conclude that bridging between these residues only occurs in the open state. Although there are apparent discrepancies between these reports, both of these bridges between S4 and S5 have robust effects on channel gating, making them ideal candidates for constraining the position and motions of the S4 helix relative to the pore if the states in which they exist and their rates of formation can be determined. Here, we explore the state dependence and kinetics of Zn^{2+} bridges between His residues at positions R362 in S4 and either F416 or A419 in S5 of the Shaker Kv channel. Our results offer a resolution to the discrepancies regarding the state dependence of binding at F416, demonstrate that the S4 helices move during the final opening transition, and constrain the distance of this motion.

MATERIALS AND METHODS

Molecular biology

DNA of Shaker H4 Kv channel, with N-type inactivation removed (IR) by deleting residues 6–46 (Zagotta et al., 1990), subcloned into a GW1-CMV expression vector (Vernalis), was provided by M. Holmgren (National Institutes of Neurological Disorders and Stroke [NINDS], National Institutes of Health, Bethesda, MD). Onto this channel background, the V369I, I372L, S376T, R362H, and A419H mutations were introduced using either standard two-step PCR or a QuikChange mutagenesis kit (Agilent Technologies), and each construct was sequenced in the NINDS core facility.

Cell culture

HEK 293 cells and Chinese hamster ovary cells were obtained from American Type Culture Collection and cultured in either Dulbecco's modified eagle medium (DMEM) or DMEM/F12 supplemented with 10 mM glucose and 10% FBS obtained from Invitrogen. On the first day after trypsination and plating onto glass microscope slide coverslips, cells were transfected using 5 µl FuGene6 (Roche) and 1–2 µg each of the appropriate Shaker channel DNA and pGreenlantern (GFP) DNA (originally from Invitrogen). Currents were recorded 20–72 h after transfection, or on occasion, cells were trypsinized 24–48 h after transfection, replated, and recorded 15–48 h later.

Electrophysiology

All experiments were preformed at room temperature (~22°C). Recording pipettes were pulled from borosilicate glass capillary tubes (model GC150F-7.5; Harvard Bioscience) using a horizontal puller (model P97; Sutter Instrument Co.). Pipette resistances ranged from 1 to 3 MΩ. Extracellular Zn^{2+} was applied using a rapid solution perfusion system (RSC 200; Bio-Logic), where 10–20-ms exchange times were obtainable with carefully positioned lifted whole cells or outside-out patches (much longer exchange times were observed when cells remained attached to coverslips).

The internal (pipette) solution contained (in mM): 160 KCl, 1 EGTA, 10 HEPES, and 0.5 $MgCl_2$, pH 7.4 with KOH. The external solution contained (in mM): 45 KCl, 100 NaCl, 10 HEPES, 0.5 MgCl, and 2 CaCl, pH 7.2 with KOH. Dilute Zn^{2+}-containing recording solutions were made fresh daily from a 1-M stock solution in H_2O (a decrease in Zn^{2+} potency was noted in dilute Zn^{2+}-containing solutions used several days after being made). Membrane voltage was controlled using a patch clamp amplifier (Axon 200B; Axon Instruments). Currents were filtered at 5 kHz (eight-pole Bessel; 900 filter; Frequency Devices, Inc.) and digitally recorded at 20 kHz using a Digidata board and pCLAMP software (both from Axon Instruments).

Data analysis

Off-line analysis was performed using both Clampfit (Axon Instruments) and Solver (Excel; Microsoft). Error bars are ±SEM. Single Boltzmann functions were fit to G-V relations using the equation $G / G_{max} = (1 + e^{-zF(V-V_{1/2})/RT})^{-1}$, where G/G_{max} is the normalized conductance determined from tail current amplitudes, z is the equivalent charge movement, $V_{1/2}$ is the half-activation voltage, F is Faraday's constant, R is the gas constant, and T is the temperature in Kelvin.

Modeling

Markov models were used for kinetic simulations. Microscopic reversibility was specifically observed. For simplicity, it was assumed that channels are either in the open (fully conducting) or closed states, with no subconductance states considered. Rate constants between states were constrained as described below, with voltage-dependent rate constants assumed to have exponential voltage dependence. Time courses describing the occupancy of each state were calculated according to the method described by Colquhoun and Hawkes (1995). In brief, the occupancy of each state at time t is given by $\mathbf{p}(t) = \mathbf{p}(0)e^{\mathbf{Q}t}$, where $\mathbf{p}(t)$ is a row vector with one element for each state in the model. $\mathbf{p}(0)$ contains the occupancy probabilities of each state at t = 0, which is calculated using the initial rate constants. The tasks of calculating rate constants, building the Q-matrix, and solving for the above equations were performed by original programs run in Mathcad 2000 adapted from those in Phillips et al. (2003).

Modeling constraints

Two-state model. To model the late opening transitions that are isolated with the ILT mutations, we initially examined how a simple two-state model consisting of an open state and a closed state separated by a single voltage-dependent transition can reproduce the control ILT channel data. All of the models shown in Fig. 7 reduce to a two-state model in the absence of Zn^{2+}. Fitting a single voltage-dependent Boltzmann function to the G-V relation in control provides a measurement of the total voltage dependence of the transition and a ratio for the forward and backward rates. By constraining the total voltage dependence of both the forward and the backward transition, and the ratio of the on-rate to the off-rate, this two-state model can reasonably describe the steady-state G-V relation in control conditions (Fig. 7 A, control). Next, the kinetics of voltage-dependent channel activation and deactivation were fit by adjusting how the total voltage dependence of the transition is distributed between opening and closing and by changing the opening and closing rates. We set values for the opening and the closing rates while keeping them at the fixed ratio that reproduces the steady-state G-V relation. With these constraints, this model provides a reasonable approximation of the kinetics of voltage-dependent channel opening and closing (Fig. 7 B, control). As is the case for all of these two-state models, the redistribution of states occupied after a voltage step occurs at a rate governed by $\tau = 1/(k_o + k_c)$, and the slowest redistribution will thus occur after a voltage step to the voltage at the midpoint ($V_{1/2}$) of the G-V curve.

Three-state model (Scheme 2). We extended the two-state model by adding a single state representing Zn^{2+} binding to the open state, with a single concentration-dependent transition. For all of the models in Fig. 7, we keep all of the rate constants determined for the two-state model in the absence of Zn^{2+} the same, adjusting only the Zn^{2+} binding and unbinding rates. By adjusting the ratio of the Zn^{2+} on-rate to the Zn^{2+} off-rate, this three-state model reproduces the steady-state G-V curves in both control and in the presence of Zn^{2+} (Fig. 7, Scheme 2, A). However, with these constraints it is not possible to reproduce the voltage-dependent opening and closing rates in the presence of Zn^{2+}. The simulated current relaxations are always too slow (Fig. 7, Scheme 2, B). Using slower rates for Zn^{2+} binding and unbinding than those shown further slows the opening and closing rates, whereas using faster Zn^{2+} on- and off-rates has no effect.

Four-state model (Scheme 3). The four-state model incorporates Zn^{2+} binding to both the pre-open (A) and open (O) states. This model has one additional free parameter compared with the three-state model, a constant (c) allowing for faster opening of Zn^{2+}-bound channels and faster Zn^{2+} binding in the open state. If c approaches 1, then Zn^{2+} does not promote channel opening (and the model is unable to reproduce the steady-state G-V curve in the presence of Zn^{2+}). As long as c is larger than ~25, then by adjusting the ratio of the Zn^{2+} on-rate to the Zn^{2+} off-rate, this model is able to reproduce the steady-state G-V relation in the presence of Zn^{2+} (Fig. 7, Scheme 3, A). This model can reproduce any particular voltage-dependent opening and closing rates in the presence of Zn^{2+}. By increasing the Zn^{2+} on- and off-rates, the voltage-dependent opening and closing rates can be made faster than any of the data. However, the shape of the relationship between opening/closing rates as function of voltage in the presence of Zn^{2+} does not fit across the entire voltage range with a single set of Zn^{2+} binding and unbinding rates. When c is larger than ~200, the shape of this relationship becomes quite steep, and if the closing rate constant is adjusted to fit the closing rate at negative voltages, the rates at positive voltages are too fast, similar to those illustrated in Fig. 7 (Scheme 4, B). As c is lowered to 100, the shape of the relationship becomes shallower, but not enough to adequately describe the data (Fig. 7, Scheme 3, B). Additionally, the predicted relaxation rates in the presence of Zn^{2+} are biphasic. As c is lowered, the amplitude of the slow phase decreases at negative voltages, becoming insignificant around −40 mV with the rate constants used. When the relaxation is approximated by fitting with a single-exponential function, this disappearance of the slow phase causes an abrupt change in the reported τ near −40 mV (Fig. 7, Scheme 3, B).

10-state model (Scheme 4). The 10-state model shown in Scheme 4 models each of the four Zn^{2+} binding sites while allowing Zn^{2+} to bind to voltage sensors in both the pre-open and the open positions. This 10-state model has the same number of free parameters as the four-state model. In the absence of Zn^{2+}, this model again reverts to the same two-state model. If c is >2.2, the 10-state model is able to reproduce the steady-state G-V in 1 μM Zn^{2+}, as shown in Fig. 7 (Scheme 4, A). With a c value of 30, the 10-state model is able to fit the opening and closing rates at negative voltages (Fig. 7, Scheme 4, B). By adjusting c and the Zn^{2+} binding and unbinding rate constants, this model can be adjusted to fit the opening rates. At lower values of c (e.g., 3.5) and with $k_b = 2 \times 10^7\ M^{-1}s^{-1}$ and $k_u = 17\ s^{-1}$, the 10-state model predicts opening and closing rates in Zn^{2+} that are biphasic, similar to that observed for the four-state model. This model also cannot fit all of the determined opening and closing rates with a single set of rate constants.

15-state model (Scheme 5). We considered a 15-state model in which the final transition of each voltage sensor can occur

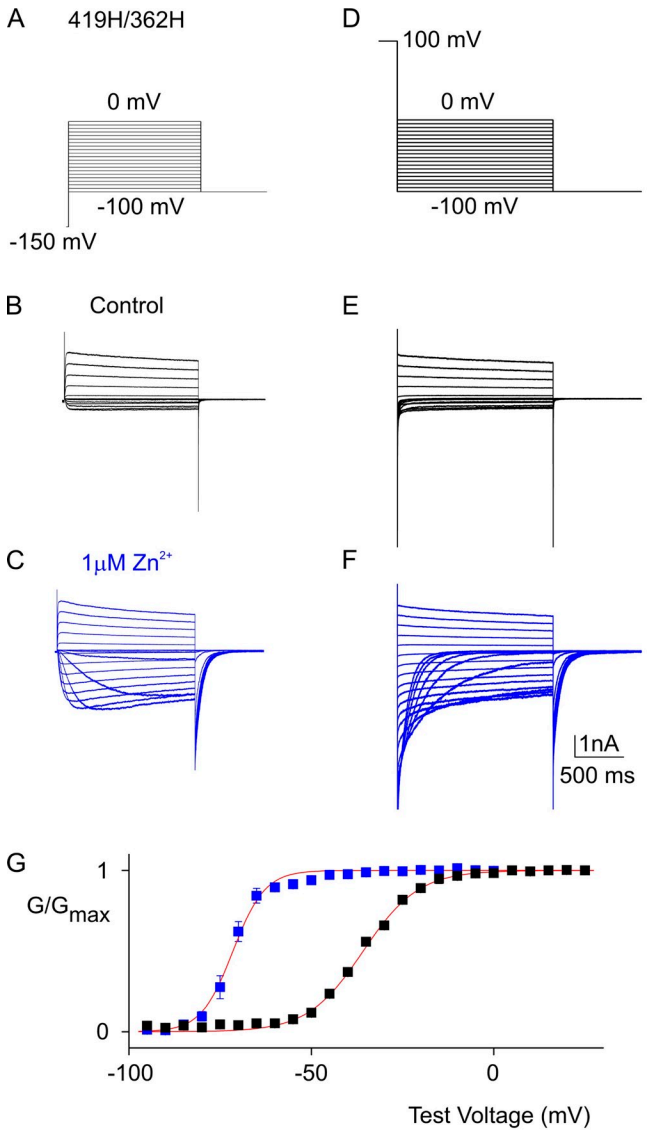

Figure 1. Zn^{2+} shifts the G-V relation of 419H/362H channels to negative voltages. Macroscopic currents from 419H/362H channels expressed in a HEK cell in either control external solution (black) or 1 μM Zn^{2+} (blue) and average steady-state conductance verses voltage relations determined from tail current measurements for a population of cells. (A) Voltage protocol illustrating 5-mV incrementing steps to voltages between −100 and 0 mV consecutively applied after an 800-ms prepulse to −150 mV. Holding voltage was −100 mV. (B) Representative macroscopic current records obtained in control solution using the protocol illustrated in A. (C) Macroscopic current traces recorded in the presence of 1 μM Zn^{2+} using the voltage protocol shown in A. (D) Voltage protocol illustrating 5-mV steps to voltages between −100 and 0 mV consecutively applied after a 100-ms prepulse voltage step to +100 mV to open the channels. (E) Representative macroscopic current records showing channel deactivation in control solution using the protocol illustrated in D. (F) Macroscopic current traces recorded in the presence of 1 μM Zn^{2+} using the voltage protocol shown in D. (G) Normalized steady-state channel conductance determined from tail current measurements after both activation (B and C) and deactivation (E and F), plotted as a function of membrane voltage. Data points are the mean normalized conductance determined after both activation and deactivation for three to four cells similar to that illustrated in A–F in either control (black) or 1 μM Zn^{2+} (blue). Smooth red curves are best fits of single Boltzmann functions to the data in Zn^{2+} ($V_{1/2}$ = −72 mV and z = 4.8) and in control ($V_{1/2}$ = −36 mV and z = 3.3).

independently, with pore opening occurring as the fourth voltage sensor moves into its open-state position. In the absence of Zn^{2+}, this 15-state model simplifies to a five-state model, in contrast to the previous schemes, which simplify to two-state models. In this five-state model, each voltage sensor is assumed to move independently. This five-state model contains the same number of free parameters as the two-state model. Similarly to the two-state model, this five-state model can reproduce the steady-state G-V in the absence of Zn^{2+} (Fig. 8, Scheme 5, A, control). Unlike the two-state model where the voltage-dependent opening and closing rates at a given voltage are the same (Fig. 7, Schemes 2–4, B, control), the five-state model predicts subtle differences between the opening and closing rates (Fig. 7, Scheme 5, B), better approximating the observed data. In the five-state model, the maximum of the relationships between opening/closing rates and voltage are both leftward shifted from the predictions of the two-state model, more closely resembling the observed channel data. We constrained the 15-state model to reproduce the opening and closing rates observed in the absence of Zn^{2+}. This 15-state model can fit the steady-state G-V relation in the presence of Zn^{2+} by adjusting the ratio of the Zn^{2+} on-rate to the Zn^{2+} off-rate (Fig. 8, Scheme 4, A). By setting appropriate values for the Zn^{2+} on- and off-rates, this model can reasonably closely reproduce how opening and closing rates vary as a function of voltage (Fig. 8, Scheme 4, B).

RESULTS

To provide constraints on the location and movement of the voltage sensors relative to the pore, we examined Shaker channels with IR (Zagotta et al., 1990) and with mutations R362H in the voltage sensor and either A419H or F416H in the pore domain. We expressed these channels in HEK cells and used either whole cell or outside-out patch recording to examine the macroscopic voltage-activated potassium currents they produce. To determine the state dependence and kinetics of Zn^{2+} bridge formation between A419H in the channel pore domain and R362H in the voltage sensor, we examined the effects of Zn^{2+} on the steady-state channel conductance from Shaker IR R362H and A419H (419H/362H) channels (Fig. 1). To assure that steady-state conductance has been reached and is not distorted by changes in the kinetics of channel activation or deactivation, channel conductance was determined from normalized tail currents after both channel activation and channel deactivation. We find that 1 μM Zn^{2+} causes a dramatic leftward shift in a plot of the average steady-state conductance verses membrane voltage (G-V curve) (Fig. 1 G), revealing that Zn^{2+} is either stabilizing the open state or destabilizing a closed state, consistent with the previous reports (Lainé et al., 2003; Lewis et al., 2008). To demonstrate that the leftward shift of the G-V curve by Zn^{2+} application is caused by Zn^{2+} being coordinated by the two introduced His residues, we examined the effects of Zn^{2+} on channels with or without single His

residues introduced. We find that unlike the effects observed with millimolar Zn^{2+} concentrations (Sack and Aldrich, 2006), 10 µM Zn^{2+} causes no appreciable changes in their G-V relationships (Fig. 2), confirming that the bridge is formed between 362 and 419.

The binding of Zn^{2+} to open channels

The effects of Zn^{2+} on the 419H/362H G-V curve occur at voltages where these channels exist in a combination of both open and closed states and therefore could result from Zn^{2+} binding to either open or closed states. Zn^{2+} binding to and stabilizing channels in the open state would be expected to slow channel closing kinetics, whereas Zn^{2+} binding to and destabilizing a closed state would speed channel opening. To distinguish between these two possibilities, we examined the effect of Zn^{2+} on the kinetics of channel opening and closing (Fig. 3). We quantified channel opening and closing rates by fitting

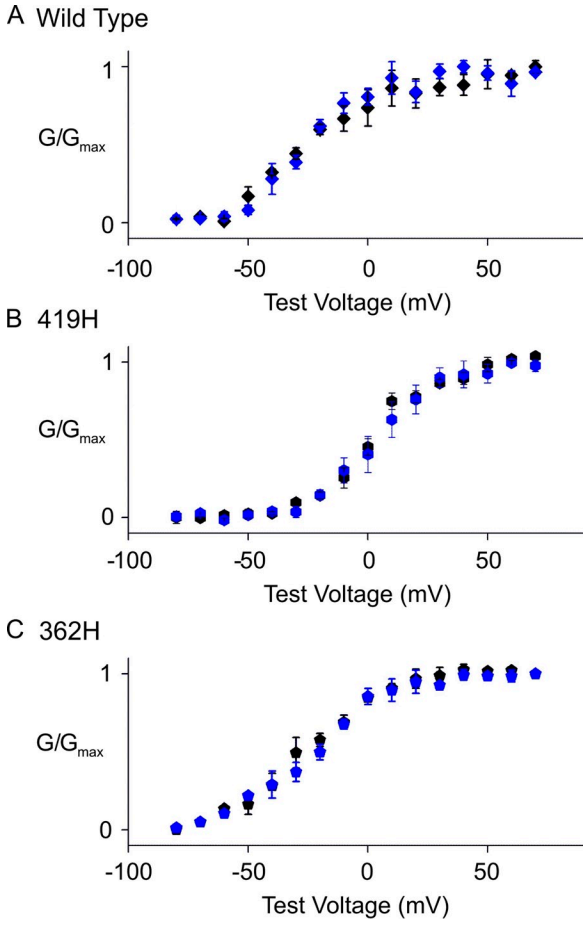

Figure 2. 10 µM Zn^{2+} has no effect on the G-V relations for control Shaker Kv channel constructs. Normalized steady-state channel conductance, as determined from tail currents, plotted as a function of membrane voltage. Each point is the average from three to six experiments. Data recorded in control are plotted as black symbols, and that recorded in 10 µM Zn^{2+} are plotted as blue symbols. (A) Wild-type Shaker IR channels, (B) A419H Shaker IR channels, and (C) R362H Shaker IR channels.

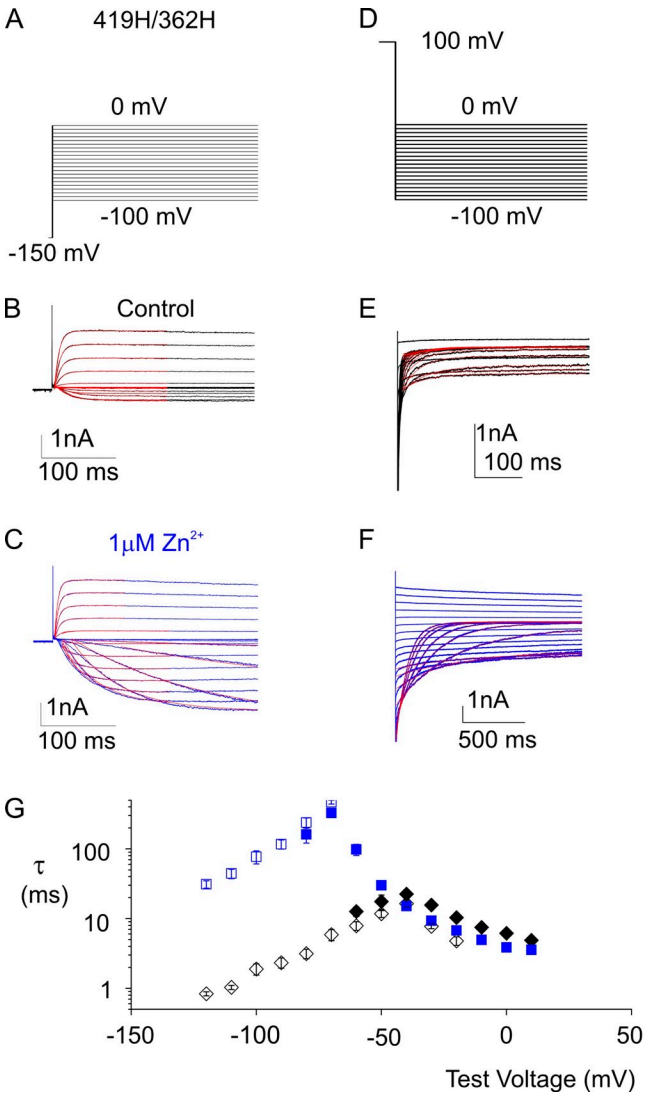

Figure 3. Zn^{2+} binds to and stabilizes 419H/362H channels in the open state. Kinetics of opening and closing for 419H/362H channels expressed in a HEK cell in either control external solution (black) or 1 µM Zn^{2+} (blue). (A) Voltage protocol for examining the kinetics of channel opening after 5-mV incrementing steps to voltages between −100 and 0 mV consecutively applied after an 800-ms prepulse to −150 mV. Holding voltage was −100 mV. (B) Representative macroscopic current records obtained in control solution using the protocol illustrated in A. (C) Macroscopic current traces recorded in the presence of 1 µM Zn^{2+} using the voltage protocol shown in A. (D) Voltage protocol for examining the kinetics of channel closing after 5-mV steps to voltages between −100 and 0 mV consecutively applied after a 100-ms prepulse voltage step to +100 mV to open the channels. (E) Representative macroscopic current records showing channel deactivation in control solution using the protocol illustrated in D. (F) Macroscopic current traces recorded in the presence of 1 µM Zn^{2+} using the voltage protocol shown in D. In B, C, E, and F, red curves are single-exponential fits to the current records after initial lags in current activation. (G) Mean time constants (τ) from single-exponential fits to channel activation (filled symbols) and deactivation (open symbols) in either control (black diamonds) or 1 µM Zn^{2+} (blue squares), plotted as a function of the voltage at which the current was recorded. $n = 3–4$ cells.

single-exponential functions to the changes in macroscopic currents observed after voltage steps (Fig. 3, B, C, E, and F, red lines). By plotting the average time constants (τ) from these single-exponential functions against the membrane voltage at which the traces were recorded (Fig. 3 G), we find that the deactivation rate (filled symbols) in Zn^{2+} (blue) is dramatically slower than in control (black), whereas the activation rate is relatively unaltered. These results indicate that Zn^{2+} binds to and stabilizes Shaker 419H/362H channels in the open state.

Preferential binding of Zn^{2+} to open compared with pre-open channels

The results thus far are consistent with the possibility that the 419H/362H Zn^{2+} bridge equally stabilizes channels in both the open state and a "pre-open" state, where S4 has already activated and the gate has not yet opened. Equal stabilization of pre-open and open states would be expected if the S4 helix did not actually move during the final opening transition. Alternatively, the Zn^{2+} bridge might stabilize the open state compared with the pre-open state, which would demonstrate that S4 moves during the final opening transition. Although it is difficult to distinguish between these scenarios in the wild-type Shaker Kv channel because the final opening transition is forward biased, the ILT mutations facilitate isolation of the pre-open state from the open state (Ledwell and Aldrich, 1999). To determine if Zn^{2+} bridges form between R362H and A419H in both pre-open and open states, we introduced the R362H and

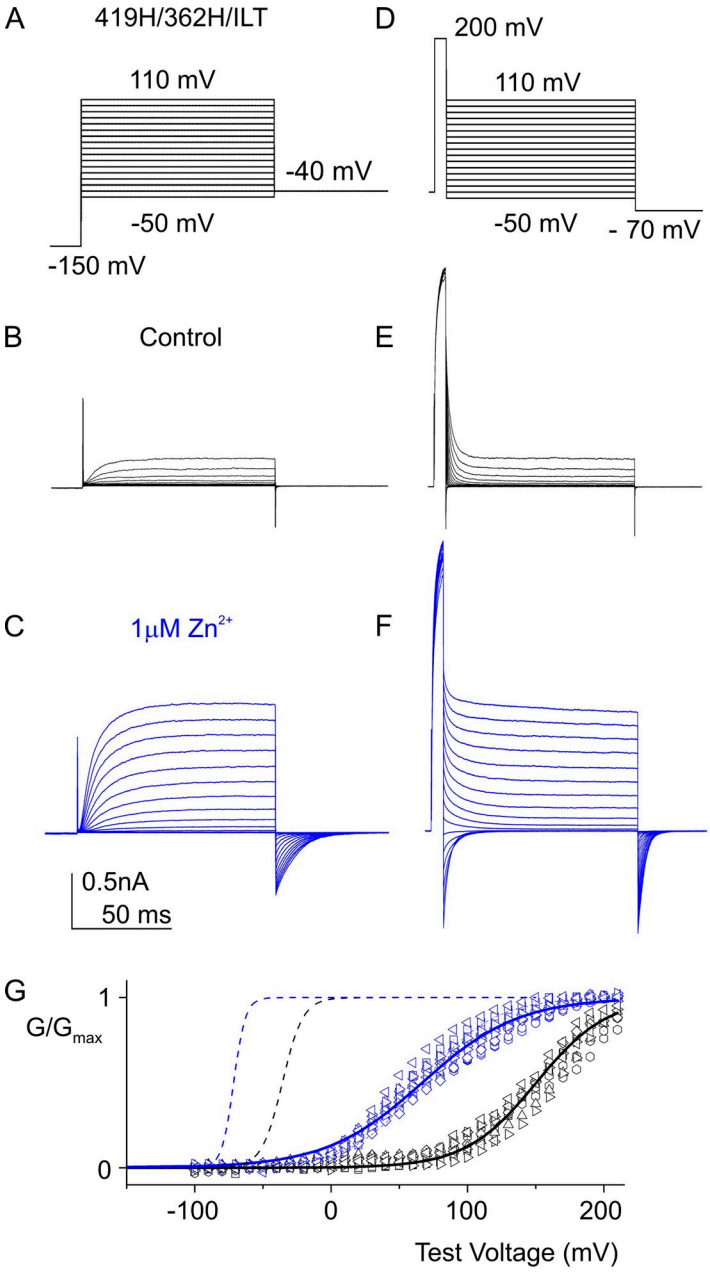

Figure 4. Zn^{2+} shifts the G-V relation of 419H/362H/ILT channels to negative voltages. Macroscopic currents from 419H/362H/ILT channels expressed in a HEK cell in either control external solution (black) or 1 μM Zn^{2+} (blue), and average steady-state conductance verses voltage relations determined from tail current measurements for a population of cells. (A) Voltage protocol illustrating 10-mV incrementing steps to voltages between −50 and +110 mV consecutively applied after a 150-ms prepulse to −150 mV. Holding voltage was −100 mV. (B) Representative macroscopic current records obtained in control solution using the protocol illustrated in A. (C) Macroscopic current traces recorded in the presence of 1 μM Zn^{2+} using the voltage protocol shown in A. (D) Voltage protocol illustrating 10-mV steps to voltages between −50 and +110 mV consecutively applied after a 12-ms prepulse voltage step to +200 mV to open the channels. (E) Representative macroscopic current records showing channel deactivation in control solution using the protocol illustrated in D. (F) Macroscopic current traces recorded in the presence of 1 μM Zn^{2+} using the voltage protocol shown in D. (G) Normalized steady-state channel conductance determined from tail current measurements after both activation (B and C) and deactivation (E and F), plotted as a function of membrane voltage. Each symbol type is from a different cell examined like the one illustrated in A–F. The G-V relation for each cell was fit with a single Boltzmann function and average values from these fits: $V_{1/2}$ = 152.6 ± 0.6 and z = 0.95 ± 0.01; n = 13 for control; $V_{1/2}$ = 66.52 ± 0.8 and z = 0.72 ± 0.08; n = 12. Solid lines are single Boltzmann functions with mean values for $V_{1/2}$ and z values. For reference, fits of single Boltzmann function to the G-V data for the non-ILT background (see Fig. 1) are plotted as dashed lines.

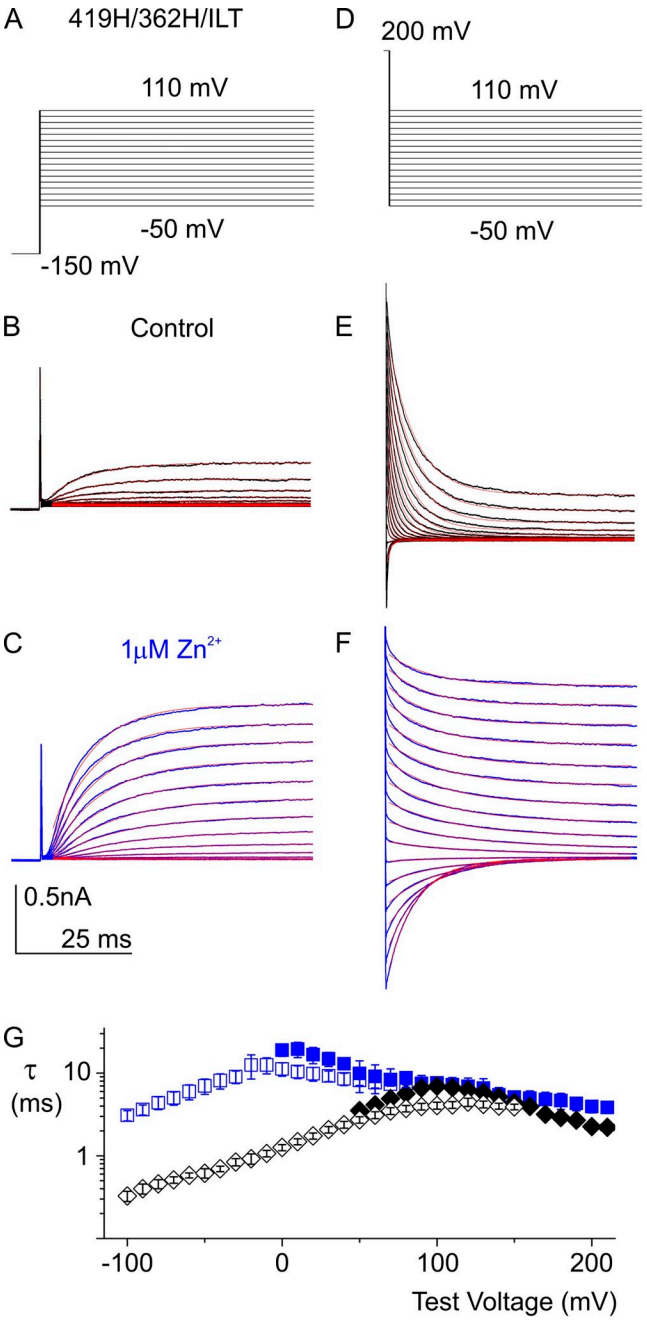

Figure 5. Zn^{2+} binds to and stabilizes 419H/362H/ILT channels in the open state. Kinetics of opening and closing for 419H/362H/ILT channels expressed in a HEK cell in either control external solution (black) or 1 μM Zn^{2+} (blue). (A) Voltage protocol for examining the kinetics of channel opening after 10-mV incrementing steps to voltages between −50 and +110 mV consecutively applied after a 150-ms prepulse to −150 mV. Holding voltage was −100 mV. (B) Representative macroscopic current records obtained in control solution using the protocol illustrated in A. (C) Macroscopic current traces recorded in the presence of 1 μM Zn^{2+} using the voltage protocol shown in A. (D) Voltage protocol for examining the kinetics of channel closing after 10-mV steps to voltages between −50 and +110 mV consecutively applied after a 12-ms prepulse voltage step to +200 mV to open the channels. (E) Representative macroscopic current records showing channel deactivation in control solution using the protocol illustrated in D. (F) Macroscopic current traces recorded in the presence of 1 μM Zn^{2+} using the voltage protocol shown in D. In B, C, E, and F, red curves are single-exponential fits to the current records after initial lags in current activation. (G) Mean time constants (τ) from single-exponential fits to channel activation (filled symbols) and deactivation (open symbols) in either control (black diamonds) or 1 μM Zn^{2+} (blue squares), plotted as a function of the voltage at which the current was recorded. n = 12–13 cells.

A419H mutations into the ILT background (forming 419H/362H/ILT channels) and used protocols similar to those in Fig. 1, adjusting voltages to accommodate the shifted voltage dependence of ILT channels (Fig. 4). Comparing the steady-state G-V curves in Fig. 4 G reveals that Zn^{2+} causes an ∼85-mV shift to more negative voltages, which is significantly larger than the 35-mV shift in the G-V curve observed in the control (non-ILT) background (Fig. 1 G, illustrated as dashed lines in Fig. 4 G). Although there is large cell-to-cell variability in the voltage dependence of opening in ILT channels (Fig. 4 G), consistent with previous studies of this mutant (Smith-Maxwell et al., 1998b), it is clear that the ILT mutations have a dramatic effect on the voltage dependence of channel opening, and that the addition of Zn^{2+} shifts the channels from the pre-open into the open state. In ILT channels containing only one or neither of the His substitutions, these concentrations of Zn^{2+} did not cause any significant shift in the G-V relations (not depicted), suggesting that Zn^{2+} bridges between 419H and 362H largely counteract the effect of the ILT mutations on the final opening transition. Examination of the effects of Zn^{2+} on the kinetics of channel opening and closing (Fig. 5) reveals that the closing rate is dramatically slower in the presence of Zn^{2+} (blue symbols) compared with control (black symbols), and that the activation rates are relatively unaffected (Fig. 5 G), similar to that observed in the 419H/362H channels (Fig. 3 G). Collectively, these results show that Zn^{2+} binds to and stabilizes 419H/362H/ILT channels in the open state relative to the pre-open state, revealing that there is movement between R362H in S4 and A419H in the pore during the final opening transition.

Kinetics of Zn^{2+} binding to open channels

Zn^{2+} coordination between 362H and 419H constrains the location of these two positions in the S4 and S5 helices because coordination can occur only in a limited number of ideal geometries and precise distances (Alberts et al., 1998). However, Zn^{2+} coordination may trap the S4 in a rarely sampled position that would not be representative of its relative position in the open state. Our next objective was therefore to explore the kinetics of Zn^{2+} bridge formation because the Zn^{2+} on-rate places a lower limit on how often the voltage sensor is located in the appropriate position for Zn^{2+} coordination. The large increase in channel current seen at some voltages

upon Zn^{2+} application to 419H/362H/ILT channels provides a convenient means of assessing the kinetics of bridge formation. When Zn^{2+} is rapidly applied to the extracellular solution, we observe rapid increases in channel current (τ = 10–100 ms; Fig. 6) that vary as functions of both voltage and Zn^{2+} concentration, indicating that the rate of bridge formation is fast. Recovery after the removal of Zn^{2+} is also rapid (τ = 30–100 ms; Fig. 6) and voltage dependent, but independent of Zn^{2+} concentration. Simulations using models incorporating four bridges per channel suggest that the underlying Zn^{2+} binding rate is likely to be $>10^7$ $M^{-1}s^{-1}$, and the Zn^{2+} unbinding rate is probably between 10 and 120 s^{-1} (Figs. 7 and 8). The rapid unbinding rate indicates that the Zn^{2+} bridge between 362 and 419 is not capable of trapping a rarely sampled conformation. The rate of metal bridge formation is more rapid than the rate of $\sim 10^6$ $M^{-1}s^{-1}$ observed for Cd^{2+} coordination within the internal pore regions of the Shaker Kv channel (del Camino and Yellen, 2001) or the P2X receptor channel (Li et al., 2010), examples where at least three Cys residues coordinate the metal ion. Collectively, the rapid binding and unbinding rates for 419H/362H channels suggest that bridging occurs in the open state, and in that state, His residues at 362 in S4 and 419 in S5 are optimally positioned to coordinate Zn^{2+}.

Can Zn^{2+} bind before channels open?

The experimental results thus far with 419H/362H channels suggest that Zn^{2+} binds rapidly to the open state and stabilizes it over the pre-open state, requiring that Zn^{2+} bind more tightly to the open state than to the pre-open state. These results do not exclude the possibility that Zn^{2+} is able to weakly bind channels in the pre-open state before the S4 helices have undergone their final movement. To explore this possibility, we consider multiple kinetic models to explain the actions of Zn^{2+} on the final opening transition of 419H/362H/ILT channels (Figs. 7 and 8). Ledwell and Aldrich (1999) found that much of their data obtained on ILT channels at positive voltages could be reproduced using a two-state model to represent the final opening transition between the pre-open and open states. We initially explored whether a simple three-state model with Zn^{2+} binding only to the open state (Fig. 7, Scheme 2) can reproduce our data for 419H/362H/ILT channels over voltage ranges that similarly focus on the final opening transition (refer to Materials and methods). As observed by Ledwell and Aldrich (1999) for ILT channels, in the absence of Zn^{2+}, both the steady-state G-V curve and the voltage-dependent activation and deactivation rates from 419H/362H/ILT channels can be reasonably well described using a single set of rates for the transition between pre-open and open states (Fig. 7, shown in black). However, this three-state model is unable to reproduce the voltage-dependent activation and deactivation

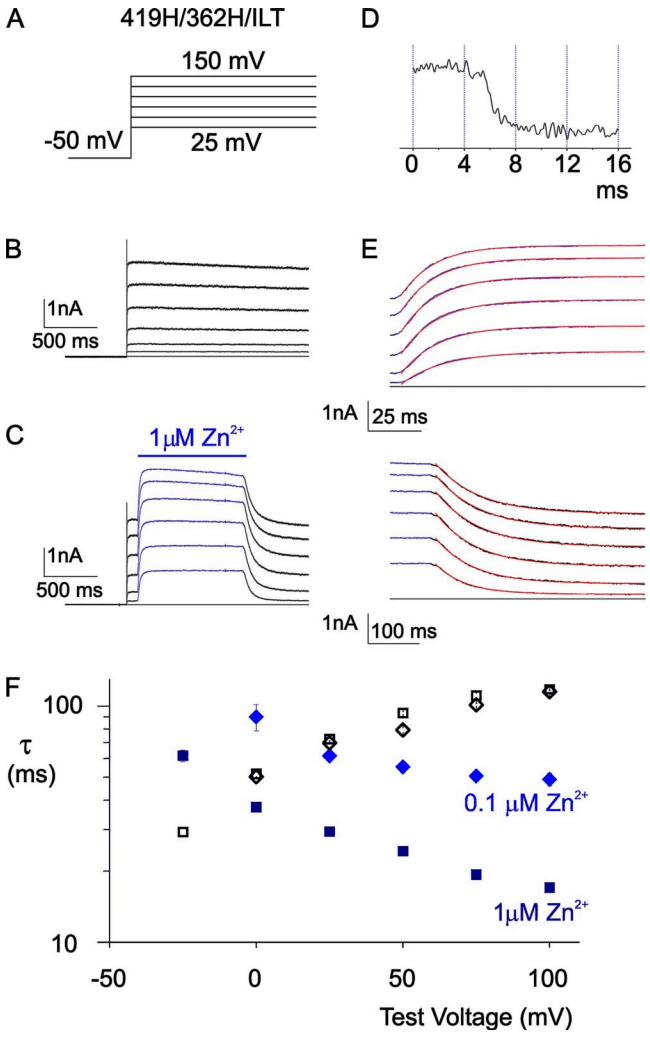

Figure 6. Rapid binding and unbinding of Zn^{2+} for 419H/362H/ILT channels. Opening of channels in response to Zn^{2+} application and closing after the removal of Zn^{2+} at different voltages. (A) Voltage protocol illustrating 25-mV steps to six different voltages between 25 and +150 mV, each consecutively applied from a holding potential of −50 mV. (B) Representative macroscopic currents recorded in response to consecutively applied voltage pulses (A), which open channels in a cell bathed continuously in control solution. (C) Representative currents where the external solution is rapidly switched from control to 1 μM zinc (same cell as in B). (D) Current record from a pipette with no patch (open tip), where the solution flowing over the pipette tip is switched between the control extracellular solution and similar solution containing 160 mM KCl, illustrating rapid solution exchange (in this case, ~4 ms). (E) Expanding view of current increases and decreases seen upon the application (above) and removal (below) of Zn^{2+} (data from C). Best fits of single-exponential functions are shown as red lines. (F) Mean time constants (τ) from single-exponential fits to changes in current upon Zn^{2+} application (filled blue symbols) or removal (open black symbols). Squares, 1 μM Zn^{2+}; n = 7–15; diamonds, 0. 1 μM Zn^{2+}; n = 4–5. Experiments were performed using both outside-out patches and whole cell recordings. There was no systematic variability in the time constants recorded in the two configurations; therefore, the data were combined.

rates in the presence of Zn^{2+}; regardless of how fast we make the Zn^{2+} binding and unbinding rate constants, the predicted voltage-dependent activation and deactivation rates in Zn^{2+} are always too slow (Fig. 7, shown in blue). We also considered a model in which Zn^{2+} can bind to the pre-open state (Fig. 7, Scheme 3), necessitating one additional free parameter, a constant that represents how much tighter Zn^{2+} binds to the open state than the pre-open state and how much faster Zn^{2+}-bound channels open. Although this model can describe the voltage-dependent activation and deactivation rates in the presence of Zn^{2+} better than Scheme 2, a single set of

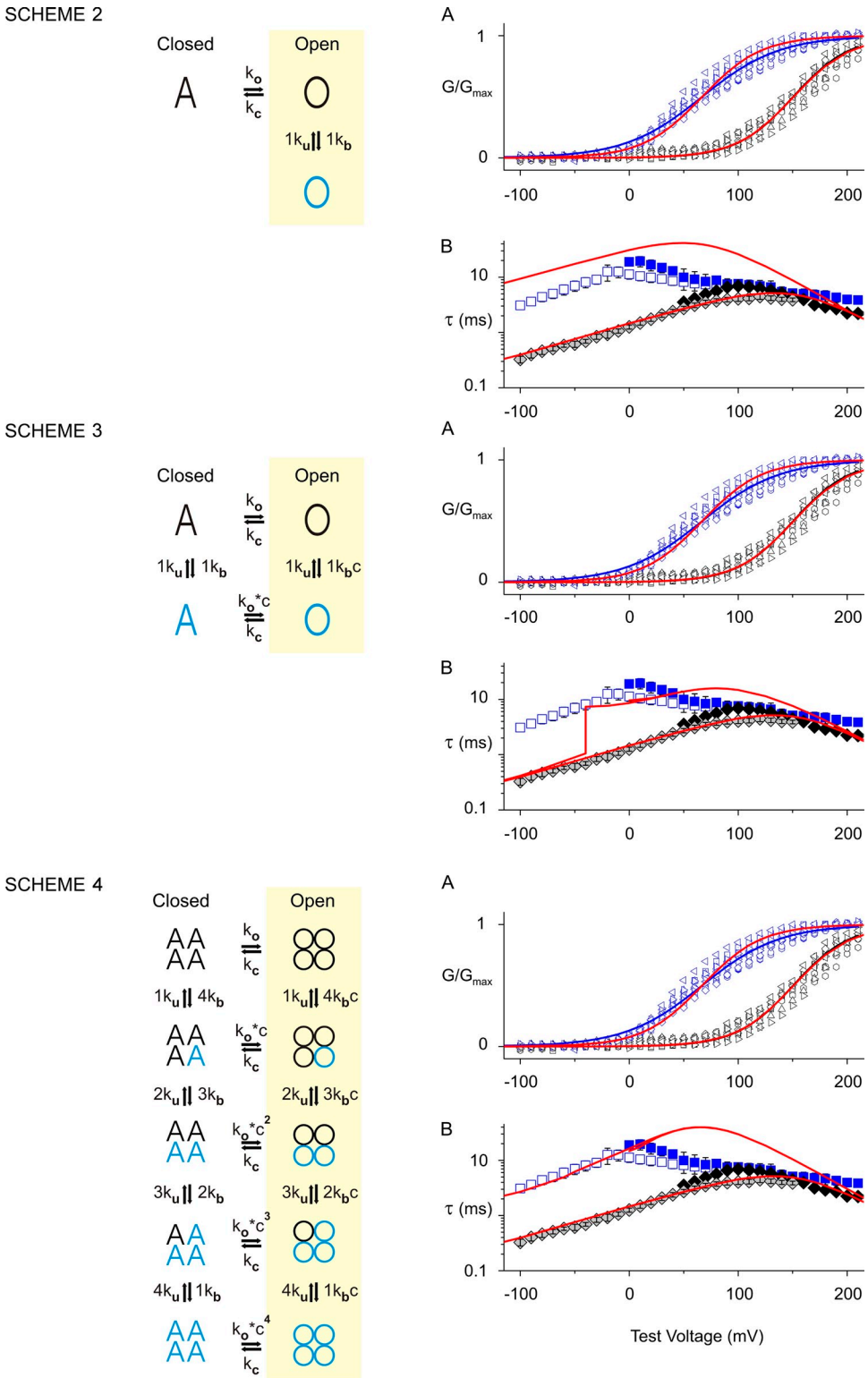

Figure 7. Kinetic models of 419H/362H/ILT channels that fail to describe gating of the channel in the absence or presence of Zn^{2+}. (Scheme 2) A three-state model in which Zn^{2+} binds to channels in the open state but not the pre-open state (O and A, respectively). (Scheme 3) A four-state model in which Zn^{2+} is allowed to bind to channels in both the open and pre-open states (O and A, respectively). (Scheme 4) A 10-state model with four independent Zn^{2+} binding sites, where Zn^{2+} can bind to channels in both the open and pre-open states (O and A, respectively). (A) Steady-state G-V relations in control (black) and 1 µM Zn^{2+} (blue) from Fig. 4 G. Model predictions are shown as red curves using the following rate constants. Scheme 2: k_o = 2.31 s^{-1} e $^{(25.2V)}$, k_c = 683 s^{-1} e $^{(12.6V)}$, k_b = 5.05 × 10^{10} $M^{-1}s^{-1}$, and k_u = 2,200 s^{-1}; Scheme 3: k_o = 2.31 s^{-1} e $^{(25.2V)}$, k_c = 683 s^{-1} e $^{(12.6V)}$, k_b = 7.5 × 10^6 $M^{-1}s^{-1}$, k_u = 100 s^{-1}, and c =100; Scheme 4: k_o = 2.31 s^{-1} e $^{(25.2V)}$, k_c = 683 s^{-1} e $^{(12.6V)}$, $k_b = 8 \times 10^6 M^{-1}s^{-1}$, $k_u = 163\ s^{-1}$, and c = 30. (B) Mean time constants (τ) from the single-exponential fits to channel activation (filled symbols) and deactivation (open symbols), plotted as a function of the voltage in either control (black) or 1 µM Zn^{2+} (blue) from Fig. 5 G. Red lines represent time constants of the best fit of single-exponential functions to the simulated current relaxations using the scheme shown to the left and the rate constants given in A. Refer to Materials and methods for further description of these models.

rate constants cannot reproduce all of the rates over the voltage range studied (Fig. 7).

The models discussed thus far are oversimplified representations of the final opening transition that is isolated with the ILT mutations because they do not take into account that each channel contains four Zn^{2+} binding sites, one between each of the four S4 and S5 helices. Scheme 4 extends the four-state model to a 10-state model by adding individual Zn^{2+} binding reactions to both the pre-open and open states (Fig. 7), but nevertheless fails to reproduce all of the activation and deactivation rates in the presence of Zn^{2+} (Fig. 7, shown in blue). In the final model we considered (Fig. 8, Scheme 5), each voltage sensor is able to move independently between a pre-open (A) and open (O) position, but Zn^{2+} can only bind after a given S4 has moved to its O position. Unlike the other models, all of which reduce to a simple two-state model in the absence of Zn^{2+}, this scheme expands the final opening transitions into four independent transitions. In each of these transitions, S4 moves between activated and "open" positions, with the channel only opening to a conducting state when the last of the four S4 helices moves into the open position. Scheme 5 better reproduces subtle features of the voltage-dependent activation and deactivation rates. These rates are not identical in the voltage range where they overlap, and their individual maxima do not occur at the midpoint of the G-V (Fig. 8), as is the case for a two-state model (see control conditions in Fig. 7). In the presence of Zn^{2+}, Scheme 5 reproduces the activation and deactivation rates better than the four- or 10-state models, even though this model has one fewer free parameter. Considering these models leads us to conclude that Zn^{2+} must bind to 419H/362H/ILT channels before the channel actually opens. Schemes 3 and 4 accomplish this by allowing Zn^{2+} to bridge before and after the final movement of the S4 helix, whereas in Scheme 5, each S4 can move independently and Zn^{2+} can bridge any given S4 (with an S5) only after it has moved into its final state. In this case, channel opening cannot occur until all of the S4 helices have moved.

A distinct bridge with Zn^{2+} binding to the pre-open state

Our next objective was to explore the state dependence of Zn^{2+} bridges between His residues introduced at R362 in S4 and F416 in S5, one helical turn below the 419

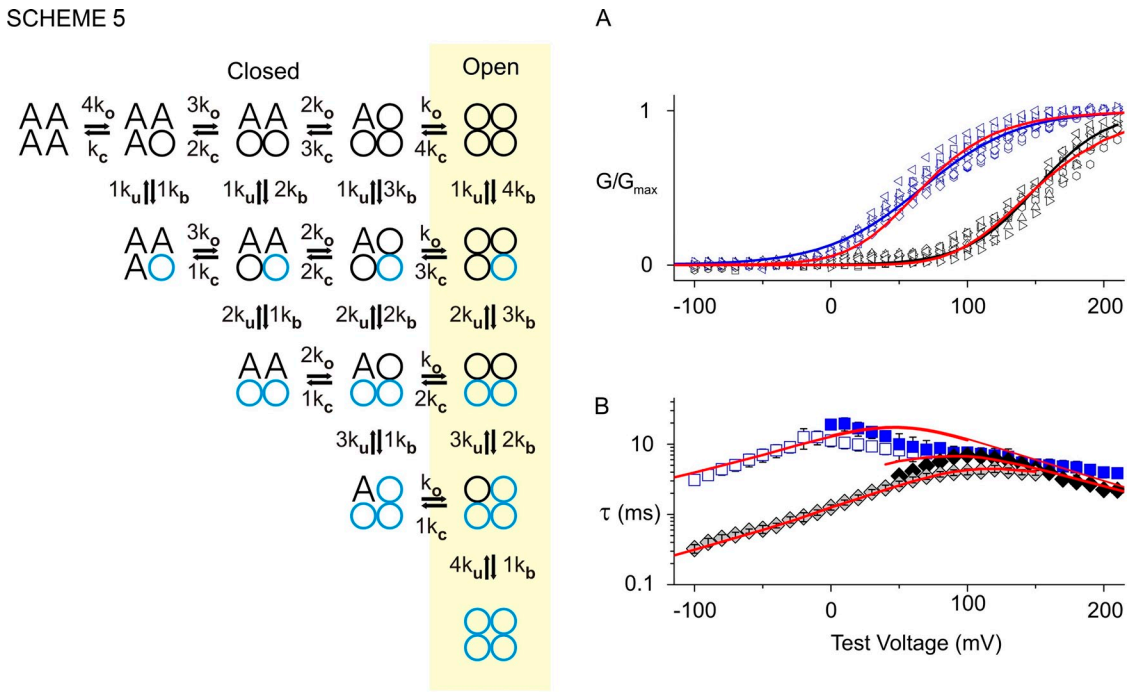

Figure 8. Kinetic models of 419H/362H/ILT data reveal that Zn^{2+} can bind before channels open. Scheme 5 is a 15-state model in which each S4 can independently move between pre-open and open positions (A and O, respectively). In this case, the channel is open (conducting) only when all four voltage sensors move into the open position, indicated by the yellow shading, and each S4 can form a Zn^{2+} bridge with S5 only after an S4 has moved to the final open position. (A) Steady-state G-V relations in control (black) and 1 µM Zn^{2+} (blue) from Fig. 4 G. Model predictions are shown as red curves using the following rate constants: $k_o = 30\ s^{-1}\ e^{(12.7V)}$, $k_c = 258\ s^{-1}\ e^{(12.6V)}$, $k_b = 1.25 \times 10^9\ M^{-1}s^{-1}$, and $k_u = 113\ s^{-1}$. (B) Mean time constants (τ) from the single-exponential fits to channel activation (filled symbols) and deactivation (open symbols), plotted as a function of the voltage in either control (black) or 1 µM Zn^{2+} (blue) from Fig. 5 G. Red lines represent time constants of the best fit of single-exponential functions to the simulated current relaxations using Scheme 5 and the rate constants given in A.

position studied thus far. Lainé et al. (2003) previously reported that Cd^{2+} bridges between Cys residues at F416 and R362 produce a slowing of opening and an apparent rightward shift in the G-V relationship, whereas Broomand et al. (2003) found that disulphide bonds between these same two Cys residues do not form when channels are held closed, but form readily when cells are repeatedly depolarized to open channels. Although this group concluded that the disulphide bond forms in the open state (Broomand et al., 2003), an alternate possibility that would be consistent with all the data is that bridges between 362 in S4 and F416 in S5 only form after the voltage sensors have activated and entered the pre-open state. The inhibitory effect in both instances could be explained if these bridges stabilize the pre-open state relative to the open state. To explore this possibility, we studied channels containing F416H and R362H mutations (416H/362H) and initially determined

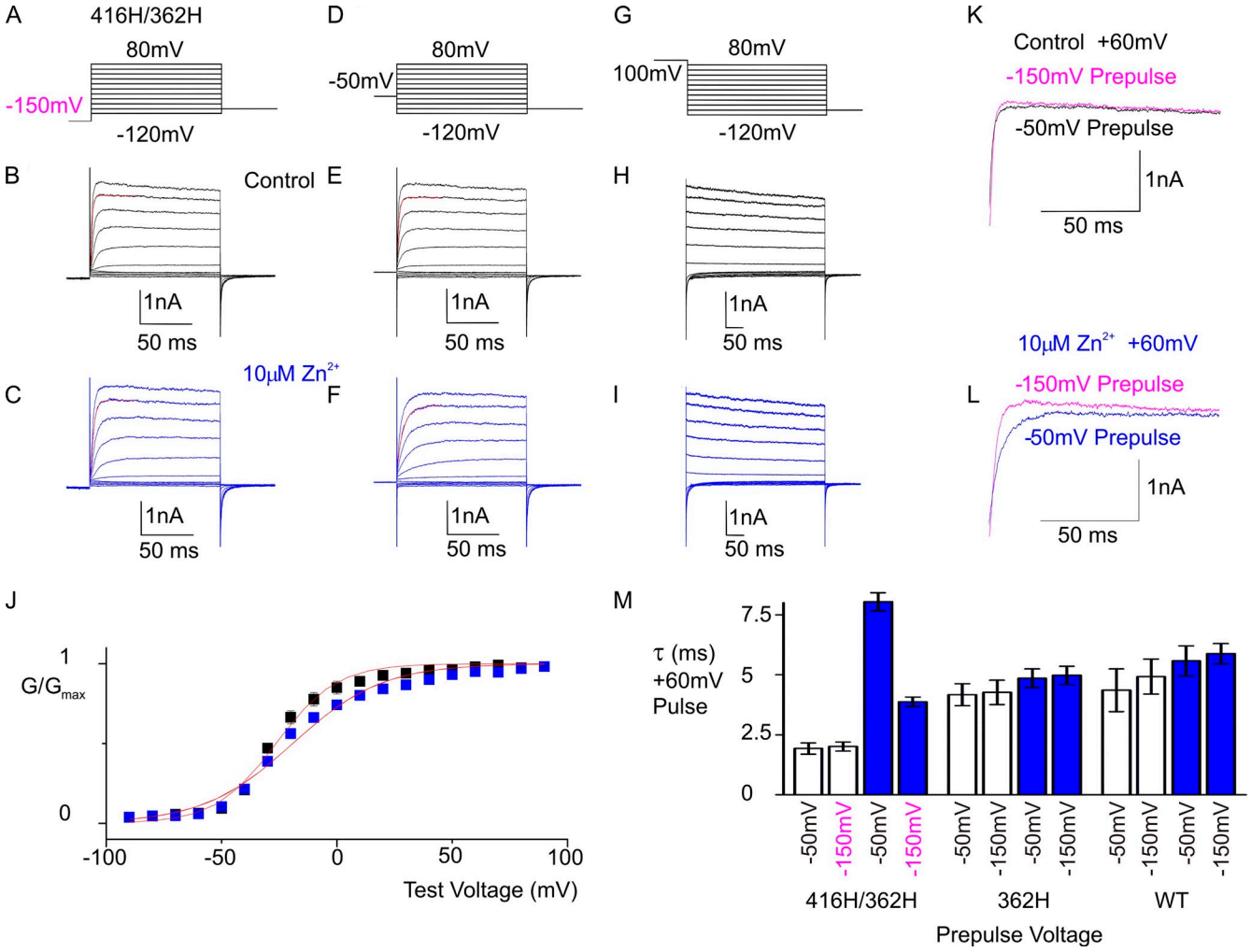

Figure 9. Zn^{2+} slows the opening of 416H/362H Shaker channels. (A and D) Voltage protocols used to investigate activation of channels when depolarizing from negative voltages (−150 mV; A) or intermediate voltages (−50 mV; D). Steps are in 20-mV increments to voltages between −120 and +80 mV, followed by a repolarizing step to −100 mV to elicit tail currents. Holding voltage was −100 mV, and the membrane voltage was stepped to either −150 or −50 mV for 400 ms before eliciting test depolarizations. (G) Protocol to study deactivation of channels after a 100-ms prepulse to +100 mV. (B, E, and H) Representative macroscopic current traces consecutively recorded from a HEK cell bathed in control solution in response to the voltage protocol shown above. (C, F, and I) Macroscopic current traces consecutively recorded from a HEK cell bathed in Zn^{2+} (10 μM)–containing solution in response to the voltage protocol shown above. The red curves in B, C, E, and F represent single-exponential fits to the current traces elicited by depolarization to +60 mV. (J) Normalized steady-state channel conductance, as determined from tail currents after both activation and deactivation, plotted as a function of membrane voltage for control (black) and 10 μM Zn^{2+} (blue). Each point is a mean conductance from four to six cells, similar to the one illustrated in A–I. Red lines are the best fits of single Boltzmann functions to the data, with $V_{1/2} = -24.5$ mV and $z = 1.75$ for control and $V_{1/2} = -21$ mV and $z = 1.51$ for 10 μM Zn^{2+}. (K and L) Comparison of macroscopic current traces elicited by a step to +60 mV from a prepulse voltage of either −150 mV (magenta) or −50 mV (black or blue) in either control (K) or 10 μM Zn^{2+} (L). (M) Bar graph of averaged τ determined from single-exponential fits to the current relaxations during pulses to +60 mV after a prepulse voltage of either −50 or −150 mV in both control and Zn^{2+} from three different channel constructs. $n = 3–6$.

G-V relations (Fig. 9 J) using tail currents obtained after steps of both activation (Fig. 9, A–F) and deactivation (Fig. 9, G–I). There is a slight weakening of the voltage dependence in the presence of 10 μM Zn^{2+} (Fig. 9, blue) compared with control (black), which results in a small rightward shift of the G-V curve at some voltages. In the presence of Zn^{2+}, the kinetics of opening from a holding potential of −50 mV are significantly slower compared with opening from −150 mV (Fig. 9, M, liter). The kinetics of opening from either voltage in control solutions are similarly rapid (Fig. 9 K), as are those for either 362H or wild-type cells in both control and Zn^{2+}

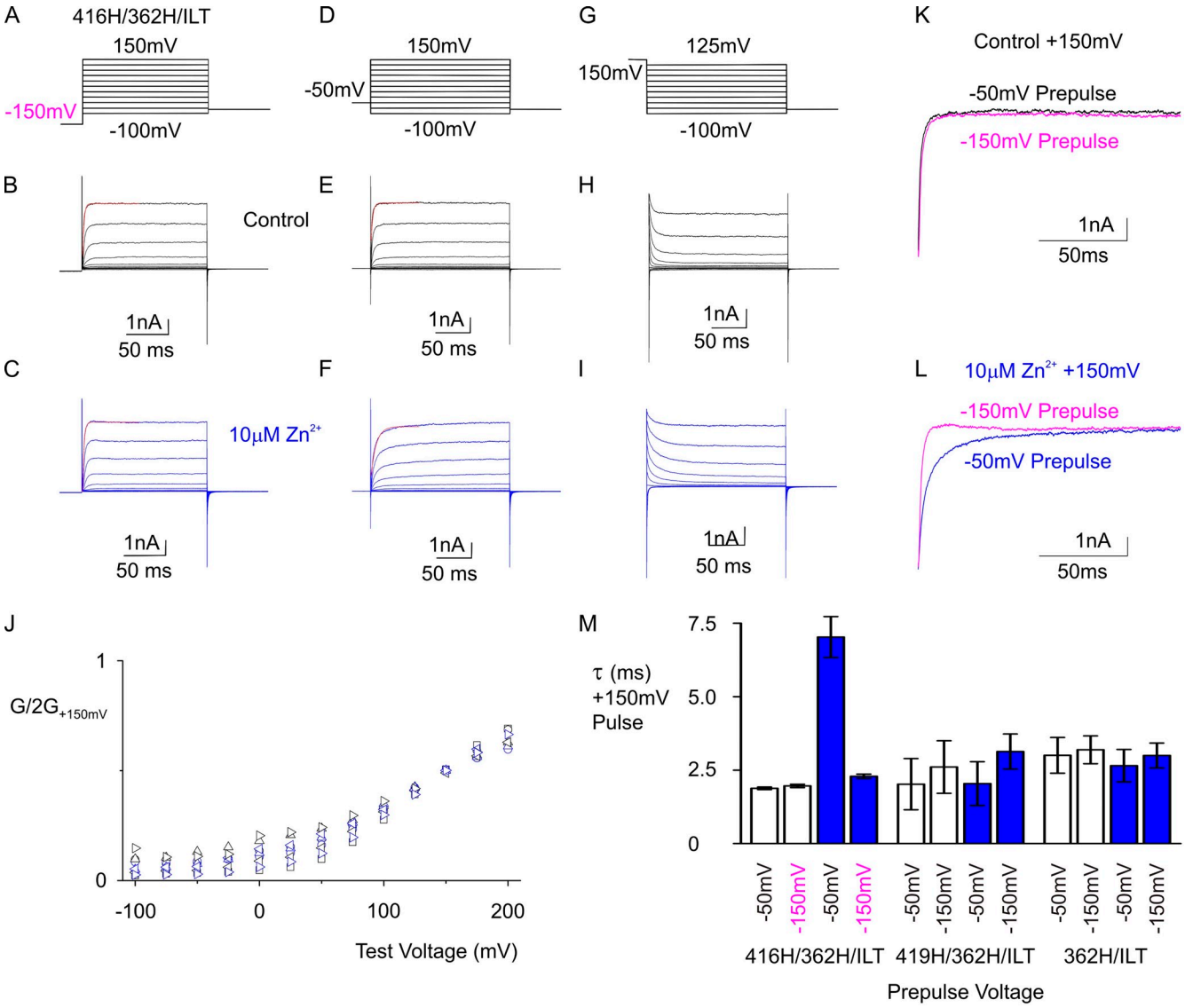

Figure 10. Zn^{2+} slows the opening of 416H/362H/ILT channels from the pre-open state. (A and D) Voltage protocols used to investigate the activation of channels when depolarizing from negative voltages (−150 mV; A) or intermediate voltages (−50 mV; D). Steps are in 25-mV increments to voltages between −100 and +150 mV, followed by a repolarizing step to −75 mV to elicit tail currents. Holding voltage was −80 mV, and the membrane voltage was stepped to either −150 or −50 mV for 200 ms before eliciting test depolarizations. (G) Protocol to study deactivation of channels after a 100-ms prepulse to +150 mV. (B, E, and H) Representative macroscopic current traces consecutively recorded from a HEK cell bathed in control solution in response to the voltage protocol shown above. (C, F, and I) Macroscopic current traces consecutively recorded from a HEK cell bathed in Zn^{2+} (10 μM)–containing solution in response to the voltage protocol shown above. The red curves in B, C, E, and F represent single-exponential fits to the current traces elicited by depolarization to +150 mV. (J) Modified measurement of steady-state channel conductance that has been normalized to the conductance at +150 mV, as determined from tail currents after both activation and deactivation, plotted as a function of membrane voltage for control (black) and 10 μM Zn^{2+} (blue). Each symbol type represents the average conductance from a single cell, like the one illustrated in A–I. (K and L) Comparison of macroscopic current traces elicited by a step to +150 mV from a prepulse voltage of either −150 mV (magenta) or −50 mV (black or blue) in either control (K) or 10 μM Zn^{2+} (L). (M) Bar graph of averaged τ determined from single-exponential fits to the current relaxations during pulses to +150 mV after a prepulse voltage of either −50 or −150 mV in both control and Zn^{2+} from three different channel constructs. n = 3–4.

(Fig. 9 M), revealing that this effect of Zn^{2+} occurs only in 416H/362H (Fig. 9 M). The fast opening rate in Zn^{2+} during steps from −150 mV is consistent with Zn^{2+} being unable to bind at −150 mV, where the voltage sensors remain in the resting state, whereas the slower opening rate in Zn^{2+} during steps from −50 mV suggests that Zn^{2+} is binding at −50 mV, where some channels are in partially activated states. The channel needs to be held at −50 mV for only 100 ms to observe slowing of opening (Fig. 9, M, liter), indicating that the rate of Zn^{2+} binding in this case is also quite rapid. Although Zn^{2+} slows opening from −50 mV, it has only small effects on the amplitude of steady-state currents at the end-test depolarizations and insignificant effects on the G-V at the most depolarized voltages, suggesting that either Zn^{2+} must unbind before the channel can open or that it stabilizes a pre-open state relative to the open state.

To distinguish whether Zn^{2+} is bridging 416H/362H in the pre-open state that is stabilized by the ILT mutations or some earlier partially activated state, we introduced the 416H/362H mutations into the ILT background. A modified G-V from 416H/362H/ILT channels that has been normalized to the conductance and +150 mV is plotted for multiple cells in Fig. 10 J, where no consistent

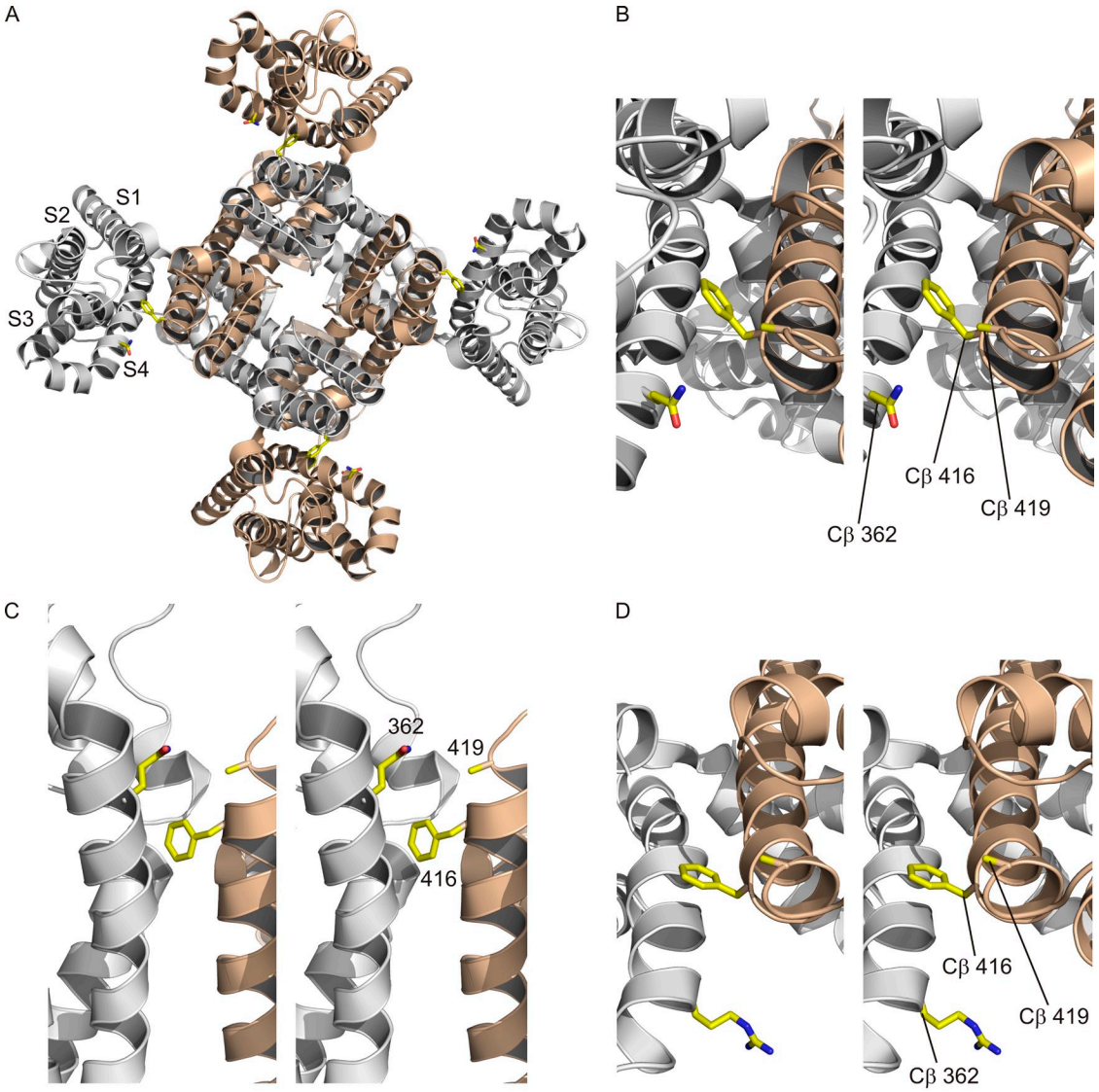

Figure 11. Bridging positions in the x-ray structures of Kv1.2 channels. (A) Ribbon representation of the Kv1.2 paddle chimera x-ray structure (Protein Data Bank accession no. 2R9R) viewed from the extracellular side of the membrane. The three residues shown with stick representations are Q290 in S4 and both F344 and A347 in S5, residues that are equivalent to R362, F416, and A419 in the Shaker Kv channel. (B) Stereo pairs of the S4 and S5 helices of the Kv1.2 paddle chimera. Same orientation as in A. (C) Stereo pairs of the S4 and S5 helices of the Kv1.2 paddle chimera viewed from the side. (D) Stereo pairs of the S4 and S5 helices of the Kv1.2 x-ray structure (Protein Data Bank accession no. 2A79) viewed from the extracellular side of the membrane as in B. The three residues shown with stick representations are R294 in S4 and both F348 and A351 in S5, residues that are equivalent to R362, F416, and A419 in the Shaker Kv channel.

effect of Zn^{2+} can be seen. These ILT-containing channels are not fully opened even at +200 mV, and without reaching the top of the G-V, it is difficult to distinguish small inhibitory effects of Zn^{2+} bridging from the variable gating properties of ILT channels (see Fig. 4 and Smith-Maxwell et al., 1998b). Nevertheless, Zn^{2+} does produce a clear slowing of channel opening when elicited by depolarizations from a holding voltage of −50 mV, where many channels are in the pre-open state, but not when elicited by depolarization from −150 mV, where the voltage sensors are in the resting state. The slow opening of ILT channels observed in the presence of Zn^{2+} from a holding voltage of −50 mV is not observed in several channel constructs lacking the F416H mutation, consistent with the effect arising from a bridge between 362 and 416. Collectively, these results suggest that Zn^{2+} bridges form between 362 and 416 in the pre-open state and stabilize that state relative to the open state.

DISCUSSION

The objective of this study was to explore the state dependence of bridges between S4 and S5 to constrain the location and motions of the S4 helix during the final opening step in the Shaker Kv channel. Our results on metal bridges formed between His residues at 362 in S4 and 419 in S5 suggest that this bridge greatly favors the open state compared with the pre-open state (Figs. 1–5), providing a clear demonstration that the S4 helix moves relative to S5 during the final opening transition. We also studied Zn^{2+} bridges between 362 in S4 and 416 in S5, and in this case our results suggest that the bridge forms when the channels enter the pre-open state after the early steps in voltage sensor activation and before the final opening transition (Figs. 9 and 10). Collectively, these results suggest that the S4 helix moves during the final opening transition from a position where a His at 362 in S4 can favorably bridge with 416 in S5 to one where 362 favorably bridges with 419. In the x-ray structure of the Kv1.2 channel, the Cβ atom of the residue equivalent to 419 is located 6.6 Å extracellular to that of the 416 equivalent, whereas in the Kv1.2 paddle chimera structure, this distance is 5.1 Å (Long et al., 2005, 2007) (Fig. 11, B–D), suggesting that the R1 position of the S4 helix moves in an extracellular direction during the final opening transition. Our results also demonstrate that the kinetics of bridge formation in the open state between 362 and 419 are rapid (Fig. 6), indicating that His residues at these positions must often be ideally positioned to coordinate Zn^{2+}. In the open Kv1.2 structure, the residue equivalent to R362 (R294) is not ideally positioned to bridge with 419 (A351 in Kv1.2), as the distance between Cβ atoms of these two residues is too long (13.7 Å) for His at these positions to coordinate Zn^{2+} (Alberts et al., 1998) (Fig. 11 D), although only a modest rotation of the S4 helix (counterclockwise viewed from outside) and movement toward S5 would be necessary to allow for optimal coordination. In contrast, the residue equivalent to R362 in the structure of the open Kv1.2 paddle chimera (R290) is positioned closer to 419 (A347 in the chimera), with a distance between Cβ atoms of 8.5 Å (Fig. 10, A–C), which is more compatible with the strict requirements for Zn^{2+} coordination (Alberts et al., 1998).

The equilibrium of voltage sensors between resting and activated states, as reflected in the gating charge (Q) versus voltage (V) relation, is sensitive to the initial voltage from which gating currents are elicited. For example, in a variety of voltage-activated channels and the Ci-VSP voltage-sensitive phosphatase, Q-V relations exhibit a pronounced shift to negative voltages when gating currents are elicited from positive voltages (Bezanilla et al., 1982; Olcese et al., 1997; Villalba-Galea et al., 2008). Villalba-Galea et al. (2008) have proposed that prolonged activation of voltage sensors at positive voltages causes them to shift into a relaxed state, and that the crystal structures of Kv channels represent this relaxed state rather than the activated state. Our constraints with bridges between S4 in both pre-open and open states are compatible with the crystal structure of the Kv1.2 paddle chimera, as discussed above, suggesting that the structural differences between activated and relaxed voltage sensors are relatively subtle and unlikely to involve a substantial repositioning of the S4 helix relative to S5.

To understand the state dependence of Zn^{2+} bridging between 362 and 419, we explored a range of kinetic models. A key conclusion that we take from these models is that the bridge can form before channels open even though the bridge ultimately stabilizes the open state (Figs. 7 and 8; and see below). Models where bridges can only form in the open state (e.g., Fig. 7, Scheme 2) poorly reproduce the observed kinetics of opening and closing in the presence of Zn^{2+}, when they are also constrained to fit the observed shift in the closed–open equilibrium evident in the G-V relations. This is because the opening and closing rates in the absence of Zn^{2+} limit how rapidly Zn^{2+} can bind and how fast the channel can close after Zn^{2+} unbinding. Models that treat the final opening transition as a single concerted motion of the four voltage sensors and gate (e.g., Fig. 7, Schemes 2–4) also cannot reproduce the observed kinetics of opening and closing even if they allow for bridging before opening of the channel. In contrast, Scheme 5 (Fig. 8) reproduces the observed kinetics of opening and closing in both the absence and presence of Zn^{2+} by allowing each voltage sensor to independently move between pre-open and open positions before the channel actually opening. These findings together imply that the final opening step defined using the ILT construct is not actually a single transition but likely involves movement of each S4 helix between pre-open

and open positions. Although Scheme 5 (Fig. 8) treats these motions of the four S4 helices as independent, there may be cooperative interactions (Pathak et al., 2005) that we have omitted for simplicity. It should also be noted that experimental conditions and variations between channel constructs can have effects on the cooperativity of individual transitions (Sack and Aldrich, 2006). The prominent lags expected for multiple transitions are not observed in ILT when activating from voltages where the voltage sensors have already undergone their initial activation (e.g., 0 mV in ILT and −50 mV in 419H/362H/ILT) because the late transitions have weak voltage dependence, and at these intermediate voltages, channels are distributed between the multiple pre-open states in Scheme 5 (Fig. 8). It is important to note that although our results clearly demonstrate voltage sensor movement during the late steps in channel opening, some of the voltage dependence observed in these late steps may result from other sources.

The emerging picture whereby the voltage sensors move in both the early activating steps and the late opening transition has several additional implications for understanding the gating mechanisms and pharmacology of voltage-dependent ion channels in a more general context. First, there are a wide variety of different ion channels that contain S1–S4 voltage-sensing domains, yet it remains unclear whether their gating mechanisms involve the equivalent of both the early and late transitions that operate within the Shaker Kv channel. The Shaw Kv channel (Kv3) appears to primarily use the equivalent of the final opening transition in Shaker (Smith-Maxwell et al., 1998a,b; Ledwell and Aldrich, 1999), providing a clear example of a channel that only uses a subset of the voltage-sensing conformation changes that are present in Shaker. It will be fascinating to explore whether S4 motions are required to gate other weakly voltage-dependent channels, including Ca^{2+}-activated potassium channels (Ma et al., 2006), cyclic nucleotide gate channels (Benndorf et al., 1999; Martínez-François et al., 2009), and TRP channels (Voets et al., 2004, 2007). Second, the two bridges studied here provide clear examples of how molecules might perturb the gating mechanisms of voltage-activated ion channels by interacting with specific conformations of the voltage sensors. Because the voltage sensors move during both the early activating steps and the late opening transition, ligands that bind to voltage sensors can potentially influence any conformation change involved in gating the channel.

We thank Miguel Holmgren, Lorin Milescu, Joe Mindell, Andrew Plested, Shai Silberberg, and members of the Swartz laboratory for helpful discussions, and the NINDS DNA sequencing facility for DNA sequencing.

This work was supported by the Intramural Research Program of the NINDS, National Institutes of Health, and a National Institute of General Medical Sciences PRAT fellowship to L.R. Phillips.

Christopher Miller served as editor.

Submitted: 12 August 2010
Accepted: 8 November 2010

REFERENCES

Alberts, I.L., K. Nadassy, and S.J. Wodak. 1998. Analysis of zinc binding sites in protein crystal structures. *Protein Sci.* 7:1700–1716. doi:10.1002/pro.5560070805

Benndorf, K., R. Koopmann, E. Eismann, and U.B. Kaupp. 1999. Gating by cyclic GMP and voltage in the α subunit of the cyclic GMP-gated channel from rod photoreceptors. *J. Gen. Physiol.* 114:477–490. doi:10.1085/jgp.114.4.477

Bezanilla, F. 2002. Voltage sensor movements. *J. Gen. Physiol.* 120:465–473. doi:10.1085/jgp.20028660

Bezanilla, F., R.E. Taylor, and J.M. Fernández. 1982. Distribution and kinetics of membrane dielectric polarization. 1. Long-term inactivation of gating currents. *J. Gen. Physiol.* 79:21–40.

Bezanilla, F., E. Perozo, and E. Stefani. 1994. Gating of Shaker K+ channels: II. The components of gating currents and a model of channel activation. *Biophys. J.* 66:1011–1021. doi:10.1016/S0006-3495(94)80882-3

Broomand, A., R. Männikkö, H.P. Larsson, and F. Elinder. 2003. Molecular movement of the voltage sensor in a K channel. *J. Gen. Physiol.* 122:741–748.

Chakrapani, S., L.G. Cuello, D.M. Cortes, and E. Perozo. 2008. Structural dynamics of an isolated voltage-sensor domain in a lipid bilayer. *Structure.* 16:398–409. doi:10.1016/j.str.2007.12.015

Colquhoun, D., and A.G. Hawkes. 1995. A Q-matrix cookbook: how to write only one program to calculate the single-channel and macroscopic predictions for any kinetic mechansim. *In* Single-Channel Recording. B. Sakmann and E. Neher, editors. Plenum Press, New York. 589–636.

Cuello, L.G., D.M. Cortes, and E. Perozo. 2004. Molecular architecture of the KvAP voltage-dependent K+ channel in a lipid bilayer. *Science.* 306:491–495. doi:10.1126/science.1101373

del Camino, D., and G. Yellen. 2001. Tight steric closure at the intracellular activation gate of a voltage-gated K(+) channel. *Neuron.* 32:649–656.

del Camino, D., M. Kanevsky, and G. Yellen. 2005. Status of the intracellular gate in the activated-not-open state of shaker K^+ channels. *J. Gen. Physiol.* 126:419–428. doi:10.1085/jgp.200509385

Hille, B. 2001. Ion channels of excitable membranes. Third edition. Sinauer, Sunderland, MA. 814 pp.

Holmgren, M., K.S. Shin, and G. Yellen. 1998. The activation gate of a voltage-gated K+ channel can be trapped in the open state by an intersubunit metal bridge. *Neuron.* 21:617–621.

Hoshi, T., W.N. Zagotta, and R.W. Aldrich. 1994. Shaker potassium channel gating. I: transitions near the open state. *J. Gen. Physiol.* 103:249–278. doi:10.1085/jgp.103.2.249

Jiang, Y., A. Lee, J. Chen, V. Ruta, M. Cadene, B.T. Chait, and R. MacKinnon. 2003. X-ray structure of a voltage-dependent K+ channel. *Nature.* 423:33–41. doi:10.1038/nature01580

Lainé, M., M.C. Lin, J.P. Bannister, W.R. Silverman, A.F. Mock, B. Roux, and D.M. Papazian. 2003. Atomic proximity between S4 segment and pore domain in Shaker potassium channels. *Neuron.* 39:467–481. doi:10.1016/S0896-6273(03)00468-9

Ledwell, J.L., and R.W. Aldrich. 1999. Mutations in the S4 region isolate the final voltage-dependent cooperative step in potassium channel activation. *J. Gen. Physiol.* 113:389–414.

Lee, S.Y., A. Lee, J. Chen, and R. Mackinnon. 2005. Structure of the KvAP voltage-dependent K+ channel and its dependence on the lipid membrane. *Proc. Natl. Acad. Sci. USA.* 102:15441–15446.

Lewis, A., V. Jogini, L. Blachowicz, M. Lainé, and B. Roux. 2008. Atomic constraints between the voltage sensor and the pore domain in a voltage-gated K^+ channel of known structure. *J. Gen. Physiol.* 131:549–561.

Li, M., T. Kawate, S.D. Silberberg, and K.J. Swartz. 2010. Pore-opening mechanism in trimeric P2X receptor channels. *Nat. Commun.* 1:1–7.

Long, S.B., E.B. Campbell, and R. Mackinnon. 2005. Crystal structure of a mammalian voltage-dependent Shaker family K+ channel. *Science.* 309:897–903. doi:10.1126/science.1116269

Long, S.B., X. Tao, E.B. Campbell, and R. MacKinnon. 2007. Atomic structure of a voltage-dependent K+ channel in a lipid membrane-like environment. *Nature.* 450:376–382. doi:10.1038/nature06265

Ma, Z., X.J. Lou, and F.T. Horrigan. 2006. Role of charged residues in the S1–S4 voltage sensor of BK channels. *J. Gen. Physiol.* 127:309–328.

Martínez-François, J.R., Y. Xu, and Z. Lu. 2009. Mutations reveal voltage gating of CNGA1 channels in saturating cGMP. *J. Gen. Physiol.* 134:151–164.

Milescu, M., J. Vobecky, S.H. Roh, S.H. Kim, H.J. Jung, J.I. Kim, and K.J. Swartz. 2007. Tarantula toxins interact with voltage sensors within lipid membranes. *J. Gen. Physiol.* 130:497–511. doi:10.1085/jgp.200709869

Milescu, M., F. Bosmans, S. Lee, A.A. Alabi, J.I. Kim, and K.J. Swartz. 2009. Interactions between lipids and voltage sensor paddles detected with tarantula toxins. *Nat. Struct. Mol. Biol.* 16:1080–1085. doi:10.1038/nsmb.1679

Olcese, R., R. Latorre, L. Toro, F. Bezanilla, and E. Stefani. 1997. Correlation between charge movement and ionic current during slow inactivation in Shaker K^+ channels. *J. Gen. Physiol.* 110:579–589. doi:10.1085/jgp.110.5.579

Pathak, M., L. Kurtz, F. Tombola, and E. Isacoff. 2005. The cooperative voltage sensor motion that gates a potassium channel. *J. Gen. Physiol.* 125:57–69.

Phillips, L.R., D. Enkvetchakul, and C.G. Nichols. 2003. Gating dependence of inner pore access in inward rectifier K(+) channels. *Neuron.* 37:953–962.

Ramu, Y., Y. Xu, and Z. Lu. 2006. Enzymatic activation of voltage-gated potassium channels. *Nature.* 442:696–699. doi:10.1038/nature04880

Sack, J.T., and R.W. Aldrich. 2006. Binding of a gating modifier toxin induces intersubunit cooperativity early in the Shaker K channel's activation pathway. *J. Gen. Physiol.* 128:119–132. doi:10.1085/jgp.200609492

Schmidt, D., and R. MacKinnon. 2008. Voltage-dependent K+ channel gating and voltage sensor toxin sensitivity depend on the mechanical state of the lipid membrane. *Proc. Natl. Acad. Sci. USA.* 105:19276–19281.

Schmidt, D., Q.X. Jiang, and R. MacKinnon. 2006. Phospholipids and the origin of cationic gating charges in voltage sensors. *Nature.* 444:775–779. doi:10.1038/nature05416

Schoppa, N.E., and F.J. Sigworth. 1998a. Activation of shaker potassium channels. I. Characterization of voltage-dependent transitions. *J. Gen. Physiol.* 111:271–294.

Schoppa, N.E., and F.J. Sigworth. 1998b. Activation of Shaker potassium channels. II. Kinetics of the V2 mutant channel. *J. Gen. Physiol.* 111:295–311. doi:10.1085/jgp.111.2.295

Schoppa, N.E., and F.J. Sigworth. 1998c. Activation of Shaker potassium channels. III. An activation gating model for wild-type and V2 mutant channels. *J. Gen. Physiol.* 111:313–342. doi:10.1085/jgp.111.2.313

Smith-Maxwell, C.J., J.L. Ledwell, and R.W. Aldrich. 1998a. Role of the S4 in cooperativity of voltage-dependent potassium channel activation. *J. Gen. Physiol.* 111:399–420. doi:10.1085/jgp.111.3.399

Smith-Maxwell, C.J., J.L. Ledwell, and R.W. Aldrich. 1998b. Uncharged S4 residues and cooperativity in voltage-dependent potassium channel activation. *J. Gen. Physiol.* 111:421–439.

Stefani, E., L. Toro, E. Perozo, and F. Bezanilla. 1994. Gating of Shaker K+ channels: I. Ionic and gating currents. *Biophys. J.* 66:996–1010.

Sukhareva, M., D.H. Hackos, and K.J. Swartz. 2003. Constitutive activation of the Shaker Kv channel. *J. Gen. Physiol.* 122:541–556. doi:10.1085/jgp.200308905

Swartz, K.J. 2004. Towards a structural view of gating in potassium channels. *Nat. Rev. Neurosci.* 5:905–916. doi:10.1038/nrn1559

Vamvouka, M., J. Cieslak, N. Van Eps, W. Hubbell, and A. Gross. 2008. The structure of the lipid-embedded potassium channel voltage sensor determined by double-electron-electron resonance spectroscopy. *Protein Sci.* 17:506–517. doi:10.1110/ps.073310008

Villalba-Galea, C.A., W. Sandtner, D.M. Starace, and F. Bezanilla. 2008. S4-based voltage sensors have three major conformations. *Proc. Natl. Acad. Sci. USA.* 105:17600–17607.

Voets, T., G. Droogmans, U. Wissenbach, A. Janssens, V. Flockerzi, and B. Nilius. 2004. The principle of temperature-dependent gating in cold- and heat-sensitive TRP channels. *Nature.* 430:748–754.

Voets, T., G. Owsianik, A. Janssens, K. Talavera, and B. Nilius. 2007. TRPM8 voltage sensor mutants reveal a mechanism for integrating thermal and chemical stimuli. *Nat. Chem. Biol.* 3:174–182. doi:10.1038/nchembio862

Webster, S.M., D. Del Camino, J.P. Dekker, and G. Yellen. 2004. Intracellular gate opening in Shaker K+ channels defined by high-affinity metal bridges. *Nature.* 428:864–868. doi:10.1038/nature02468

Xu, Y., Y. Ramu, and Z. Lu. 2008. Removal of phospho-head groups of membrane lipids immobilizes voltage sensors of K+ channels. *Nature.* 451:826–829. doi:10.1038/nature06618

Yellen, G. 2002. The voltage-gated potassium channels and their relatives. *Nature.* 419:35–42.

Zagotta, W.N., T. Hoshi, and R.W. Aldrich. 1990. Restoration of inactivation in mutants of Shaker potassium channels by a peptide derived from ShB. *Science.* 250:568–571.

Zagotta, W.N., T. Hoshi, and R.W. Aldrich. 1994a. Shaker potassium channel gating. III: evaluation of kinetic models for activation. *J. Gen. Physiol.* 103:321–362. doi:10.1085/jgp.103.2.321

Zagotta, W.N., T. Hoshi, J. Dittman, and R.W. Aldrich. 1994b. Shaker potassium channel gating. II: transitions in the activation pathway. *J. Gen. Physiol.* 103:279–319. doi:10.1085/jgp.103.2.279